BEND PROPAGATION IN FLAGELLA

II. Incorporation of Dynein Cross-Bridge Kinetics into the Equations of Motion

Michael Hines and J. J. Blum, *Department of Physiology, Duke University Medical Center, Durham, North Carolina 27710 U.S.A.*

ABSTRACT The cross-bridge formalism of T. Hill has been incorporated into the nonlinear differential equations describing planar flagellar motion in an external viscous medium. A stable numerical procedure for solution of these equations is presented. A self-consistent two-state diagram with curvature-dependent rate functions is sufficient to generate stable propagating waves with frequencies and amplitudes typical of sperm flagella. For a particular choice of attachment and detachment rate functions, reasonable variation of frequency and wave speed with increasing viscosity is also obtained. The method can easily be extended to study more realistic state diagrams.

INTRODUCTION

In a preceding paper (Hines and Blum, 1978, hereafter referred to as I), a set of equations was derived describing the motion of a flagellum in a viscous medium in terms of the effective shear forces generated by the internal mechanisms. In that paper the shear force due to the dynein cross-bridge system was specified by a simple function of curvature with a time delay. Use of this simple and purely formal representation of the dynein system allowed us to develop a stable procedure for numerical solution of the nonlinear differential equations. This permits us to proceed to the next phase of the biophysical analysis of wave propagation in flagella, i.e., to apply the mechanochemical formalism devised by Hill (1974) to the dynein cross-bridge system.

Several studies involving the attachment and detachment of dynein cross-bridges have been published by Brokaw. In the first of these studies (Brokaw, 1975*a*), the active moment was generated by attachment and detachment functions which depended on curvature but not on shear displacement. In a subsequent paper (Brokaw, 1975*b*), the force-velocity behavior of a two-state distance-dependent rate function for attachment and detachment was investigated, but this was not introduced into a model for generation of bending waves in a viscous medium. Instead, a formally similar model with active moment taken as a function of shear rate was used (in conjunction with internal viscous resistances to stabilize the numerical computations) to generate bending waves.

Subsequently, Brokaw (1976*a*, *b*) developed a stochastic method for computing the force developed by a population of dynein arms. Frequencies of oscillation of a two-filament model were obtained for several kinds of attachment-detachment rate functions, but the dyneins were not inserted into a model for a flagellum in a viscous medium, and thus no studies on bend propagation were performed. The stochastic method follows the history

of a large number of individual dyneins, and is thus computationally expensive. Furthermore, as will be discussed below, this method introduces error terms proportional to $v^3\Delta t^2$, where v is proportional to the velocity of sliding. Thus for the large sliding velocities in flagella, very small steps of Δt are required for numerical accuracy. More recently, Brokaw and Rintala (1977) have studied more complicated diagrams for the dynein arms to assess the ATP dependence of frequency. These studies (using the stochastic procedure described above) indicated that at least a three-state diagram is necessary to obtain reasonable ATP dependence of the frequency of oscillation of the two-filament system. Thus up to the present no studies have been performed in which dynein arms modeled according to a self-consistent Hill formalism (Hill, 1974; Hill et al., 1975) have been embedded in a flagellum in a viscous medium. In this paper we extend our previous results by adding a Hill-type cross-bridge dynein system to the computer simulation procedure previously developed (I).

Because naive addition of a dynein formalism to our previous simulation procedure generates serious problems of numerical stability and accuracy, it was necessary to extend that procedure. This paper provides a full description of a simulation procedure applicable to any Hill-type cross-bridge system.

We also use the newly developed method to show that propagated bending waves are generated using a two-state diagram when the attachment and detachment functions depend on curvature in a simple way. As it turns out, even this oversimplified model generates a surprising similarity to the observed dependence of frequency and wave speed on viscosity.

A preliminary account of this work was presented at the 6th International Biophysics Congress in Kyoto, Japan, and at the Symposium on Mechanisms and Controls of Prokaryotic and Eukaryotic Flagellar Motility in Hakone, Japan, in September 1978.

DYNEIN SYSTEM FORCE GENERATION

Geometrical Considerations

In this section we derive a general treatment, suitable for use with the formalism of Hill (1974) for computing S_d, the effective shear force for a dynein cross-bridge system. Dynein arms, located on subfiber A of the i^{th} filament, are separated by a distance d_{arm}. Attachment sites, located on subfiber B of the $i + 1^{\text{th}}$ filament, are separated by a distance d_{att} (Fig. 1). We define x_{ipq} as the arc length distance between the point of insertion of the p^{th} dynein arm on filament i and the q^{th} attachment site on the adjacent filament $i + 1$. In the plane of bending, the separation between the i^{th} and the $i + 1^{\text{th}}$ filaments is $y_i - y_{i+1}$. The rate of change of x due to sliding is given by

$$dx_{ipq}/dt = (y_i - y_{i+1})\,d\gamma/dt, \tag{1}$$

where we have used the plane sections remain plane hypothesis (Lubliner and Blum, 1971) and $\gamma(s, t)$ is the effective shear between filaments. This presupposes that dynein p and attachment site q are close enough to arc length positions so that the effect of curvature in this equation is negligible.

Inasmuch as a dynein arm can only be attached in a relatively narrow range of x values,

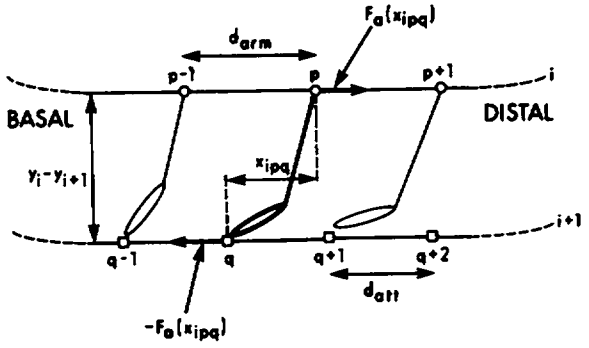

FIGURE 1 Geometrical arrangement of dynein arms and attachment sites. A pair of filaments in the plane of bending with positive curvature is shown. Dynein p on the A-subfiber of filament i is attached to attachment site q on subfiber B of filament $i + 1$. X_{ipq} is shown positive and will increase for positive sliding, i.e., filament i moving in the distal direction. Arrows are drawn to indicate the direction of positive shear force. Note that if a dynein produces a force, $F_a = -k_d x_{ipq}$ when attached, the resultant shear force is negative and moves the $i + 1$ filament in the distal direction.

we can assume that the probability of attachment $p_{ipq}(x_{ipq})$, can be >0 only when $d < x_{ipq} < d_+$. It is convenient to restrict ourselves to a single site assumption, i.e., that two dyneins cannot compete for the same attachment site and a single dynein cannot be influenced by more than one attachment site at a single time. (Generalization to multiple attachment sites is possible [Hill, 1975].) The single site assumption is then expressed by $d = d_+ - d_- < \min(d_{arm}, d_{att})$.

Let $F_a(x_{ipq})$ be the force produced along the i^{th} filament when the p^{th} dynein on filament i is attached to the q^{th} attachment site on filament $i + 1$ and $p_{ipq}(x_{ipq})$ be the probability that the dynein arm is in fact attached. Because we will later average over an ensemble of dyneins within a small region of the flagellum, we term the average shear force produced by this dynein arm as

$$S_{ipq} = F_a(x_{ipq}) p_{ipq}(x_{ipq}). \tag{2}$$

According to the electron micrograph studies of Sale and Satir (1977) and Warner and Mitchell (1978), dyneins normally point toward the basal end of a filament when unattached and generate a distally directed force on the attached filament when attached. To be consistent with this we suppose that the significant attachment probabilities occur at positive x values and that an attached dynein generates an elastic restoring force tending to reduce x. The filament from which a dynein arises thus moves basally, whereas the filament to which it attaches moves distally. The effective shear force due to all the dyneins in the region between s and $s + \Delta s$ (where s is arc length along the flagellum) is obtained from Eq. 22*b* of Hines and Blum (I).

$$S_d(x, t) = \sum_p \sum_q \sum_{i=1}^{9} \frac{(y_i - y_{i+1})}{\Delta s} S_{ipq}, \tag{3}$$

where the sums over p and q are taken within the region s to $s + \Delta s$. We now suppose that Δs is large enough to contain a substantial population of dyneins so that we may approxi-

mate the discrete distribution of arms and sites by a continuous distribution. The average shear force per dynein contributed by the dyneins in the region from s to $s + \Delta s$ is $(1/\Delta s) \int_s^{s+\Delta s} F_a(x_{ipq}) P_{ipq}(x_{ipq}) \mathrm{d}s$. The sums over p and q yield factors of $\Delta s/d_{\mathrm{arm}}$ and $\Delta s/d_{\mathrm{att}}$, respectively. Eq. 3 thus becomes

$$S_d(s,t) = \sum_{i=1}^{9} 2 \frac{\Delta s}{d_{\mathrm{arm}}} \frac{\Delta s}{d_{\mathrm{att}}} \frac{(y_i - y_{i+1})}{\Delta s} \frac{1}{\Delta s} \int_{d_-}^{d_+} F_a(x) P_i(x) \mathrm{d}x, \tag{4}$$

where we have used the fact that the probability of attachment is nonzero only within $d_- < x_{ipq} < d_+$. The factor of 2 is due to the presence of both outer and inner arms on a microtubule.

Eq. 4 treats each filament pair separately and is computationally expensive. Computation time (and hence cost) can be reduced considerably by application of the procedure previously used for the radial link system (I; see also Brokaw, 1977). The approximation proceeds by lumping filament pairs into two systems, one having $\dot{x} > 0$, the other $\dot{x} < 0$ when $\dot{\gamma} > 0$. This utilizes the notion that dyneins on n separate filaments moving in the same direction but with different speeds have an average behavior describable as n times the force produced by a single dynein filament moving at the average speed. We thus separate Eq. 4 into two parts, one containing all terms with $(y_i - y_{i+1}) > 0$ (symbolized by $\sum^+$), the other containing all terms with $(y_i - y_{i+1}) < 0$, $(\sum^-)$.

$$S_d(s,t) = \frac{2}{d_{\mathrm{arm}} d_{\mathrm{att}}} \left\{ \left[\sum^{+} (y_i - y_{i+1}) \int_{d_-}^{d_+} F_a(x) P_i(x) \mathrm{d}x \right] + \left[\sum^{-} (y_i - y_{i+1}) \int_{d_-}^{d_+} F_a(x) P_i(x) \mathrm{d}x \right] \right\}. \tag{5}$$

For simplicity, $P_i(x,s,t)$ has been abbreviated as $P_i(x)$.

Fig. 2 shows a section perpendicular to the plane of bending. Adjacent doublets are separated by a distance h, and $y_i - y_{i+1} = h \sin(2\pi i/9) + \phi)$, where ϕ is a phase angle. As drawn in Fig. 2, filament pairs 2-3, 3-4, and 4-5 have the greatest separation in the plane of bending. Thus these three pairs are the major contributors to the sliding force for this system, and we average their contributions. Similarly, we average the contributions of the 6-7, 7-8, and 8-9 pairs for the second system. Then each sum in Eq. 5 can be approximated as $(h + 2h\cos 40^\circ)/3 \simeq 0.85\,h$. Alternatively, because $y_i - y_{i+1} = \sin(2\pi i/9 + \phi)$, one can obtain an average value for $y_i - y_{i+1}$ for all positive values of $y_i - y_{i+1}$ by integrating over the range of argument values, 0 to π. The average value of $y_i - y_{i+1}$ is then

$$\overline{y_i - y_{i+1}} = \frac{h}{\pi} \int_0^{\pi} \sin\theta d\theta = \frac{2h}{\pi} \simeq 0.64\,h.$$

Thus we approximate the nine filaments in Eq. 5 by two equivalent systems of four-filament pairs, each separated by 0.75 h, and an average probability of P_{I} for system I and P_{II}

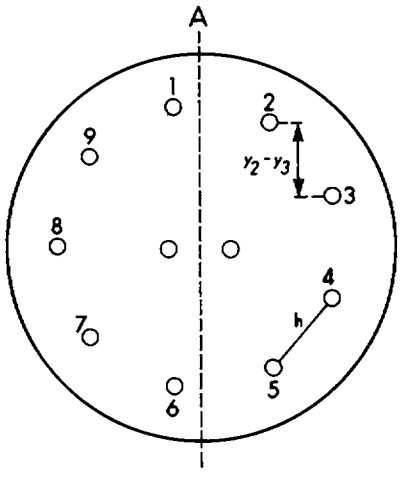

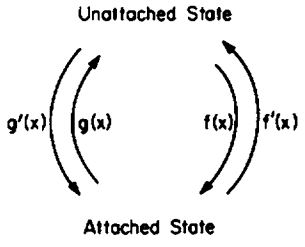

FIGURE 2

FIGURE 3

FIGURE 2 Distribution of doublets within a flagellum. A cross-section of a flagellum is shown with the plane of bending indicated by a dashed line. Each doublet is symbolized by a circle and is numbered so that a dynein originating in subfiber A of filament i may attach to an attachment site on subfiber B of filament $i + 1$, i.e., the view is from base to tip.

FIGURE 3 A self-consistent two-state diagram for attachment and detachment of cross-bridges.

for system II. Eq. 5 is then replaced by

$$S_d(s, t) = \frac{2 \cdot 4 \cdot 0.75h}{d_{\text{arm}} d_{\text{att}}} \int_{d_-}^{d_+} F_a(x)[P_{\text{I}}(x) - P_{\text{II}}(x)]\,\mathrm{d}x, \tag{6}$$

with $\dot{x} = 0.75h\dot{\gamma}$ for system I and $\dot{x} = -0.75h\dot{\gamma}$ for system II.

Dynein State Diagram

Given any state diagram specifying the mechanochemical cycle of a cross-bridge system, one can write the probabilities that the bridge will be in any particular state in terms of first-order rate constants for transitions between appropriate states (Hill, 1974). Although evidence suggests that 30S dynein can exist in at least three conformational states (Blum and Hayes, 1977), we here confine ourselves to examining the simplest possible diagram, i.e., a two-state system (Fig. 3; see also Brokaw, 1976*a*, Fig. 1). For this diagram

$$\mathrm{d}P_i(x)/\mathrm{d}t = (f(x) + g'(x))(1 - P_i(x)) - (f'(x) + g(x))P_i(x). \tag{7}$$

Because $\mathrm{d}P_i(x)/\mathrm{d}t = \partial P_i(x)/\partial t + (\mathrm{d}x/\mathrm{d}t)(\partial P_i(x)/\partial x)$, one can use Eq. 1 to obtain

$$\frac{\partial P_i(x)}{\partial t} + (y_i - y_{i+1})\dot{\gamma}\frac{\partial P_i(x)}{\partial x} = F(x) - G(x)P_i(x), \tag{8}$$

where $F(x) = f(x) + g'(x)$ and $G(x) = f(x) + f'(x) + g(x) + g'(x)$. Using the two-system approximation described above, Eq. 8 then becomes

$$\frac{\partial P_{\text{I}}(x)}{\partial t} + 0.75h\dot{\gamma}\frac{\partial P_{\text{I}}(x)}{\partial x} = F(x) - G(x)P_{\text{I}}(x) \tag{9a}$$

$$\frac{\partial P_{II}(x)}{\partial t} - 0.75h\dot{\gamma}\frac{\partial P_{II}(x)}{\partial x} = F(x) - G(x)P_{II}(x). \tag{9b}$$

Specification of the rate functions for attachment and detachment allows solution of Eqs. 9a and 9b and thus the computation of the total effective dynein shear force from Eq. 6. Clearly, generalization to three or more states poses no difficulty.

Numerical Analysis

Equations describing flagellar motion in an external viscous medium have been derived (I). These equations and the appropriate boundary conditions for a flagellum are collected here for convenience:

$$\partial^2 F_N/\partial s^2 = C_N \partial\alpha/\partial t - (1 + C_N/C_T)(\partial F_T/\partial s)(\partial\alpha/\partial s) + (C_N/C_T)F_N\partial\alpha/\partial s)^2 - F_T\partial^2\alpha/\partial s^2, \tag{10}$$

$$\partial^2 F_T/\partial s^2 = (1 + C_T/C_N)(\partial F_N/\partial s)(\partial\alpha/\partial s) + (C_T/C_N)F_T(\partial\alpha/\partial s)^2 + F_N\partial^2\alpha/\partial s^2, \tag{11}$$

$$F_N = E_b\partial^2\alpha/\partial s^2 + S_r + S_d, \tag{12}$$

where S_r is the effective shear force contributed by the radial link and nexin systems, and S_d is the effective shear force due to the dynein systems, to be obtained from Eqs. 6, 9a, and 9b. F_N and F_T are the normal shear force and tension, respectively, α is the angle of the flagellum relative to an axis fixed in the medium, and C_N and C_T are the normal and tangential viscous resistance coefficients, respectively. The boundary conditions are

$$F_N(0, t) = F_N(L, t) = 0 \tag{13a}$$

$$F_T(0, t) = F_T(L, t) = 0 \tag{13b}$$

$$M(0, t) = -E_b\left.\frac{\partial\alpha}{\partial s}\right|_{s=0} = 0; M(L, t) = -E_b\left.\frac{\partial\alpha}{\partial s}\right|_{s=L} = 0 \tag{13c}$$

$$\int_0^L (S_r(s, t) + S_d(s, t))ds = 0, \tag{13d}$$

where $M(s, t)$ is the bending moment.

Inextensibility of the filaments (Warner and Satir, 1974) also implies that

$$\frac{\partial\alpha}{\partial s} = \frac{\partial\gamma}{\partial s} \text{ [i.e. } \gamma(s, t) = \alpha(s, t) + [\gamma(0, t) - \alpha(0, t)]]. \tag{13e}$$

In the previous paper, the shear force due to the radial link plus nexin system was taken as

$$S_r = -A_1\gamma[1 - 1/\sqrt{1 + 0.75\gamma^2}] \tag{14}$$

with A_1 a constant (see Eq. 31a of I), and we continue to use this expression for S_r even though it may be more appropriate to treat the radial links as a cross-bridge system (Warner and Satir, 1974). A general computational procedure was developed in the previous paper for the solutions of Eqs. 10–14, and it remains now to introduce Eqs. 6 and 9 in a stable fashion into the system.

The variables in Eqs. 10–14 are advanced from time t to time $t + \Delta t$ by evaluating those

equations at time $t + 0.5\Delta t$, as described earlier (I). Consequently, it is necessary to evaluate S_d also at time $t + 0.5\Delta t$, which in turn makes it necessary to compute $P(x, s, t + 0.5\Delta t)$ for systems I and II. Computation with Eqs. 9 can be most easily achieved by a fully implicit method. We will discuss this issue in more detail shortly, but for the present it is sufficient to note that evaluation of Eqs. 9a and 9b requires knowledge of $\gamma(s, t + 0.5\Delta t)$, since $\dot{\gamma}$ in Eq. 9 must be computed from the relation: $\dot{\gamma}(s, t + 0.5\Delta t) = [\gamma(s, t + 0.5\Delta t) - \gamma(s, t)]/0.5\,\Delta t$. To avoid introducing another stability criterion proportional to $\Delta t/\Delta s^2$, the computation of the probabilities and of S_d is placed within the iterative procedure described in Appendix B of I in exactly the same manner as for the radial link force. The dynein shear force to be used in the matrix equation, which will be solved to obtain the $j + 1^{st}$ approximation to γ at $t + 0.5\Delta t$, is broken into a constant part and a variational part

$$S_d^{j+1} = K_s^j \gamma^{j+1} + S_K^j. \tag{15}$$

Here γ^{j+1} is the $j + 1^{st}$ successive approximation to $\gamma(s, t + 0.5\Delta t)$, K_s^j is the linear variation in the numerical computation of $S_d(s, t + 0.5\Delta t)$ with respect to $\gamma(s, t + 0.5\Delta t)$ about γ^j, and $S_K^j = S_d(\gamma^j) - K_s^j \gamma^j$, all at $t + 0.5\Delta t$. Symbolically, we write the variation as $K_s^j = \delta_\gamma S_d$. Clearly, variation of S_d in Eq. 6 is due only to variation of the probabilities, i.e., $\delta_\gamma S_d = (6h/d_{\text{arm}} d_{\text{att}}) \int_{d_-}^{d_+} F_a(x)[\delta_\gamma P_{\text{I}} - \delta_\gamma P_{\text{II}}]dx$. The linear variation of P_{I} with γ can be obtained directly from Eq. 9a (remembering that quantities not at $t + 0.5\Delta t$ do not vary) as

$$(1/\Delta t)\delta_\gamma P_{\text{I}} + 0.75h[\dot{\gamma}(\partial/\partial x)(\delta_\gamma P_{\text{I}}) + (1/0.5\Delta t)(\partial P_{\text{I}}/\partial x)] = -G(x)\delta_\gamma P_{\text{I}}. \tag{16}$$

Except for a negative sign in front of the $0.75h$, the same equation is obtained for $\delta_\gamma P_{\text{II}}$ from Eq. 9b.

At this point a comment on the form of Eq. 9 will help clarify the computational procedure chosen. Because the evaluation of γ by Eqs. 10–14 is correct to order Δt^2, $\dot{\gamma}$ is correct only to order Δt. Clearly, a high-order accuracy computation of $P(x, s, t)$ in Eq. 9 is not possible because the accuracy of the final result is limited by the order of accuracy of $\dot{\gamma}$. It is thus most efficient (as well as most stable) to use a first-order, fully implicit method for numerical solution of Eq. 9, and this is correct to order $\Delta t + v\Delta x$, for small v. For large v, the error is asymptotically proportional to $\Delta x/\Delta t$ (see Appendix A).

An alternative approach to the solution of Eq. 9 is to retain the total derivative, i.e.,

$$\mathrm{d}P(x, s, t)/\mathrm{d}t = F(x) - G(x)P(x, s, t). \tag{17}$$

In this approach, x is not held constant but the path of each dynein in the population must be followed in detail throughout the computation. The stochastic method of Brokaw (1976*a*) is one way of computing with the total derivative. It can be shown, however (see Appendix A), that the adverse effects of $\dot{\gamma}$ are still present but to a worse degree. For $\dot{\gamma} > \Delta x/\Delta t$ computations become very inaccurate. In the simulations presented in the Results, $\dot{\gamma}$ averages to about Δx per time step, Δt, but ranges up to about $10\Delta x$ per Δt.

We now proceed to evaluate the probabilities P_{I} and P_{II} (Eq. 9) and their variations with γ (Eq. 16) by means of finite difference equations. Because the left-hand side of Eq. 9

describes the transport of dynein sites relative to attachment sites, it is convenient to define $v = \pm 0.75h[\gamma(t + \Delta t) - \gamma(t)]/\Delta t$, the plus sign being used for system I, the minus sign for system II. Stable computation of equations with transport terms requires that the form of the difference equation used depends on the sign of v, i.e., the integration with respect to x must proceed in the direction of the motion. To first order in Δx and in Δt (i.e., a fully implicit method) the left-hand side of Eq. 9a when $v > 0$ can be written as

$$\frac{\partial P_I(x,t)}{\partial t} + v\frac{\partial P_I(x,t)}{\partial x} = \frac{P_I(x,t+0.5\Delta t) - P_I(x,t-0.5\Delta t)}{\Delta t} + v\frac{P_I(x,t+0.5\Delta t) - P_I(x-\Delta x,t+0.5\Delta t)}{\Delta x}. \quad (18a)$$

The boundary condition is $P_I(x = d_-, t) = 0$. Similarly, when $v < 0$

$$\frac{\partial P_I}{\partial t} + v\frac{\partial P_I}{\partial x} = \frac{P_I(x,t+0.5\Delta t) - P_I(x,t-0.5\Delta t)}{\Delta t} - v\frac{P_I(x,t+0.5\Delta t) - P_I(x+\Delta x,t+0.5\Delta t)}{\Delta x} \quad (18b)$$

with the boundary condition $P_I(x = d_+, t) = 0$. (Note that in Eq. 18 the argument s has been omitted for simplicity.) Similar equations are used for $P_{II}(s,x,t)$ (Eq. 9b) and for $\delta_\gamma P_I(x,s,t)$ and $\delta_\gamma P_{II}(x,s,t)$ (Eq. 16). In the program, the region within $d_- < x < d_+$ is divided into $NN + 1$ intervals of length Δx. Rate functions and hence the probabilities $P_I(s,x,t)$ and $P_{II}(s,x,t)$ are defined on the points $d_- + k\Delta x$, $k = 1 \cdots NN$. In the j^{th} iteration the integral in Eq. 6 is computed as

$$S_d^j(s,t+0.5\Delta t) = \frac{6h\Delta x}{d_{arm}d_{att}}\sum_{k=1}^{NN} F_a(d_- = k\Delta x)[P_I^j(d_- + k\Delta x) - P_{II}^j(d_- + k\Delta x)]. \quad (19)$$

A similar integration is used to evaluate $\delta_\gamma S_d$.

Stripped of its mathematical complexity, the numerical analysis procedure can be summarized as follows. Given a shape at time t (defined by the values of $\alpha_i (i = 2 \cdots N)$) and the probabilities $P_{I,ik}$ and $P_{II,ik}$ $(i = 2 \cdots N,\ k = 1 \cdots NN)$, at time $t - 0.5\Delta t$, one desires to advance the solution to $t + 0.5\Delta t$ by solving for the N unknown $\alpha_i(t + 0.5\Delta t)$ and the $2 \times N \times NN$ unknown probabilities at time $t + 0.5\Delta t$ and the unknown sliding, $\gamma_1(t + 0.5\Delta t) - \alpha_1(t + 0.5\Delta t)$ at the base. A first approximation to $P_{ik}(t + 0.5\Delta t)$ is found by using $(\gamma_i(t) - \gamma_i(t - \Delta t))/\Delta t$ for the velocity at $t + 0.5\Delta t$ in Eqs. 18a and 18b. These probabilities, along with the shear contributions of the radial link system and other nonlinear terms and their variations, are used to obtain the matrix terms proportional to γ as described in I, Appendix B. At the same time, the terms of the matrix equations not proportional to γ are evaluated, and the matrix equation is then solved, yielding a first approximation to $\alpha_i(t + 0.5\Delta t)$. This first approximation is then used to compute a second approximation to $P_{ik}(t + 0.5\Delta t)$ and then through the matrix equation to obtain a second approximation to $\alpha_i(t + 0.5\Delta t)$. The iteration is continued until the $P_{ik}(t + 0.5\Delta t)$ and the $\alpha_i(t + 0.5\Delta t)$ no longer change. (For the simulations used in this paper, two iterations were

sufficient.) The $\alpha_i(t + 0.5\Delta t)$ are then advanced to $\alpha_i(t + \Delta t)$ using the equation $\alpha_i(t + \Delta t) = 2\alpha_i(t + 0.5\Delta t) - \alpha_i(t)$. Because the iterative procedure is fully implicit and the advancement of $\alpha_i(t + 0.5\Delta t)$ to $\alpha_i(t + \Delta t)$ is explicit, the computational procedure for the α_i is effectively Crank-Nicolson, and thus in principle accurate to order $(\Delta t)^2$. However, because the probabilities were calculated by a fully implicit method, and thus correct to order Δt, the entire solution is now accurate only to order Δt. This is the price we pay for unconditional stability of the numerical procedure for large velocities of sliding.

RESULTS

Choice of Parameters

C_N was taken as 0.005 pN s/μm^2 for water, with $C_T = 0.5\ C_N$, and the flagellar length was taken as 30 μm.

In the previous paper (I) it was shown on structural grounds that E_b was probably in the range of 0.4–40 pN/μm^2, computed using the stiffness of elastin and collagen, respectively. It was also shown that E_b helped determine the number of waves on the flagellum. For the simulation in this paper we take $E_b = 25$ pN/μm^2 consistent with a relatively stiff filament and yielding about two waves on the flagellum.

The previous paper also computed the elastic shear coefficient A_1 to be 65 pN (per radian) under the assumption of an elastic radial link system with a Young's modulus of elastin. It turns out that reasonable dynein systems cannot generate the force necessary to overcome this elastic resistance and cause the observed amount of sliding. For the simulations in this paper the proper amount of sliding occurs when A_1 is taken as 15 pN. This may imply that elastic resistance to shear is localized primarily in the nexin links. The separation between dynein arms, d_{arm}, was taken as 24 nm (Gibbons, 1977). We have taken the distance, h, between adjacent doublets to be ~40 nm, a compromise between the center-to-center distance between adjacent doublets and the distance between a B-subfiber and its adjacent A-subfiber. Unattached dynein arms appear to tilt at an angle of about 30° basally from the vertical (Sale and Satir, 1977; Warner and Mitchell, 1978), so d must be greater than about 20 nm. Because d_{att} is likely to be a multiple of 8 nm, we chose d_{att} to be 24. The cross-bridge force constant, k_d, cannot be chosen independently of the rate functions but its value must be derived from considerations of the energy available from hydrolysis of ATP and the free energy of attachment of a dynein.

Choice of Rate Functions

Specification of the two-state cross-bridge model was initially motivated by Fig. 1 of Brokaw (1976*b*) and the pertinent discussion therein. Consistency has been maintained when changes in the rate functions (or the associated values of the dynein force constant) were investigated. As pointed out by Hill (1974), choice of a two-state diagram may be so far removed from the minimum diagram that the attachment and detachment functions used here are best regarded as empirical composites of the real rate constants in the real diagram. Our primary objective in this paper is to illustrate the use of the Hill formalism in a flagellum and to obtain some preliminary insights into the kinds of rate functions that may be useful. Extension of the present formalism to more realistic dynein diagrams is straightforward and is left for future studies.

After some preliminary trials, the rate functions chosen for investigation were

$$f(x) = f_0 e^{-0.128(x-10)^2} \tag{20a}$$

$$g(x) = g_0(1 + 1.5e^{-0.34x}) \tag{20b}$$

with $F_a = -1.6(x - x_0)$, where x (in nm) varies from d_- to d_+. This dynein system is fairly similar to Brokaw's (1976*b*) for $f_0 = 180\ s^{-1}$, $g_0 = 10\ s^{-1}$, $x_0 = 0$, $d_- = -10$ nm, and $d_+ = 10$ nm. The numbers 0.128 and 0.34 in the exponential terms of Eqs. 20*a* and 20*b* were chosen to obtain the general shape of Brokaw's rate functions.

The free energy of hydrolysis of ATP ($\Delta \cdot kT$ in Brokaw's [1976*b*] notation) is close to 100 pN · nm. A reasonable value for the difference in free energy between the lowest point on the free energy curve of the attached state and the free energy of the unattached state after hydrolysis of the ATP ($\Gamma' kt$ in Brokaw's notation) is 17.5 pN nm. This choice ensures that $g'(x)$ will be very small for $d_- < x < d_+$. The quantities Δ and Γ' along with the dynein force constant, k_d, then specify the inverse rate functions $f'(x)$ and $g'(x)$ through the relations

$$f'/f = \exp\{-(\Delta kT - \Gamma' kT - 0.5k_d(x - x_0)^2)/kT\} \tag{21a}$$

and

$$g'/g = \exp\{-(\Gamma' kT + 0.5k_d(x - x_0)^2)/kT\}. \tag{21b}$$

Note that there is a steep rise in $f'(x)$ near the location of the peak of the attachment rate at $x = d_+ = 10$ nm. Thus the attachment probability is negligible beyond d_+.

With these values for the parameters, the flagellum (after the transients subsided) oscillated synchronously around a node at its center; no propagated waves were obtained. We next introduced a simple control mechanism by making the rate functions dependent on curvature: for $\kappa > 0$, the rate functions were as specified in Eqs. 20. For $\kappa < 0$, $f(x) + g'(x) = 0$ and $g(x) + f'(x) = g_-$, i.e., when the curvature is negative, the probability of attachment is zero and detachment occurs at a constant rate, g_-, within a d region. (Note: It is assumed in the single-site hypothesis that when an attached dynein moves out of the d region [i.e. to an x value $>d_+$ or $<d_+$], it instantaneously detaches.) We initially chose $g_- = 100\ s^{-1}$. With these parameters, stable propagating waves were obtained with $\Delta t = 0.0002$ s, $N = 40$, and NN (the number of different subpopulations at constant x of dyneins within a d region) equal to 24. Snapshops of the waves obtained (after the transients have subsided) are shown in Fig. 4, panel A. Before studying the effects of changing any of these parameters, it was important to establish whether the same curves would be generated if the computational parameters were varied. In panel B, N was increased from 40 to 80, i.e. Δs was decreased from 0.75 to 0.375 μm. There were no significant differences in wave shape or wave speed. (The small differences noticeable are entirely accounted for by the changed influence of the boundary conditions, as discussed earlier [I].) Panel C of Fig. 4 shows that when NN was increased from 24 to 49, so that the number of discrete values of x at which different subpopulations of dynein arms occurred was doubled, there was again no significant change in waveform or wave speed. Decreasing Δt from 0.2 to 0.1 ms (panel D) also was without appreciable effect on wave shape or speed. Finally, increasing the number of iterations per time step (ITER) from 2 to 5 was without effect

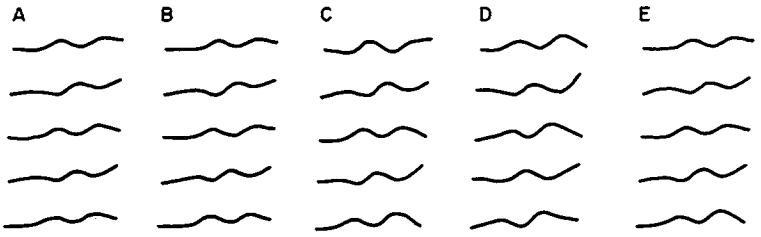

FIGURE 4 Effect of computational parameters on wave shape. Snapshots of flagellar shape computed at intervals of 0.01 s during steady wave propagation are presented using the rate functions described in the text. The first snapshot of each sequence begins at the top of each panel. Computational parameters were: $N = 40$, $NN = 24$, $\Delta t = 0.2$ ms, and ITER (the number of iterations per time step) = 2, except that in panel B, $N = 80$, in panel C, $NN = 49$, in panel D, $\Delta t = 0.1$ ms, and in panel E, ITER = 5.

(panel E). Clearly, then, numerically stable simulations with acceptable accuracy are computed with $NN = 24$, $\Delta t = 0.2$ ms, ITER = 2, and $\Delta S = 0.75$ μm. These computational parameters were used for all subsequent work.

In this first set of simulations, the amplitude was lower and the frequency was higher than usually observed in sperm (see Brokaw, 1966). To decrease the frequency, we multiplied f_0, g_0, and g_- by a factor of 0.75, and to increase the amplitude we shifted x_0, the position at which an attached arm produces zero force, to -7.65 nm, so that attachment is likely only for positive values of x. Also, the width of the d region was increased to 24 nm to allow attachment over the largest possible region consistent with d_{arm}. The steep rise in $f'(x)$ is kept near the location of the peak of the attachment rate at $x = 12$ nm by reducing k_d to 0.4 pN/nm. These rate functions are shown in Fig. 5.

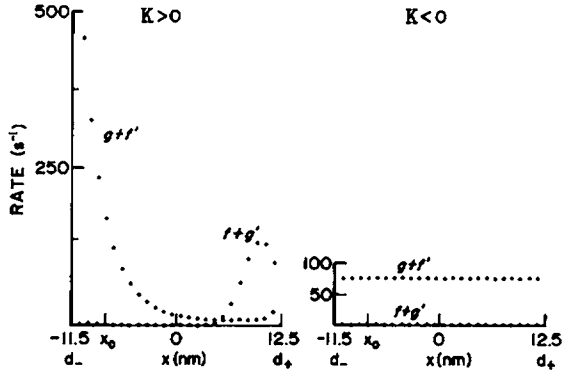

FIGURE 5 Attachment and detachment rate functions,

For $\kappa > 0$ $f(x) = 135e^{-0.128(x-10)^2}$ $\quad f'(x) = f(x)e^{(-82.5+A)/4.2}$

$g(x) = 7.5(1 + 1.5e^{-0.35x})$ $\quad g'(x) = g(x)e^{(-17.5-A)/4.2}$

with $A = 0.4(x - 7.64)^2/2$

For $\kappa < 0$ $f(x) + g'(x) = 0$

$g(x) + f'(x) = 75$

Each dot is at the particular value of x for which the probabilities of each dynein subensemble were computed. In this example (and unless otherwise specified), $NN = 24$. By definition, the probabilities of attachment are zero at d_+ and d_-, spaced one unit of Δx outside the computed range for the rate functions.

Before going on to examine flagellar motion with these parameters, it is instructive to examine the probabilities of attachment at constant sliding velocities and the force-velocity curve for positive curvature of the dynein arms. To do this, we solve Eqs. 6 and 9 at constant $\dot{\gamma}$. Fig. 6 A shows the steady-state probabilities of attachment, $P(x, t = \infty)$ as a function of x for various velocities of sliding. At positive velocities the dynein arms are approaching the attachment region from the left. Because of the shape of the attachment function (see Fig. 5), $P(x, \infty)$ is low until the arms are well along the way toward d_+, and the faster the rate of sliding the less the probability of attachment. For negative velocities, the arms approach the attachment region from the right. At d_+, $P(d_+, t) = 0$ by the single-site hypothesis. As soon as the arms enter the attachment region, however, $P(x, \infty)$ is very high, and as they move toward d_-, $P(x, \infty)$ decreases. With increasing negative speed of sliding, the maximum probability of attachment decreases and the peak broadens. A force-velocity curve (Fig. 6 B) is generated by integrating each curve according to Eq. 6 (with $P_{II}(x) = 0$) and plotting the resulting value against the velocity. Note that there is appreciable force at zero velocity and that the peak force occurs at negative velocity. The other dynein system, when active, produces a mirror image of this force-velocity curve.

Fig. 7 shows the effect of changing the size of Δx and of Δt on the transient behavior of the probabilities of attachment and of the force generated for positive curvature. Initially, the dyneins were in the zero velocity state. At $t = 0$ a constant shear velocity of -40 rad/s was imposed. Probability profiles are shown at 5-ms intervals until the new steady state is reached for two values of Δx and for two values of Δt. The dynein shear force is also plotted as a function of time. Although changing Δx from 0.96 to 0.48 nm (*NN* going from 24 to 49) changes the probability distribution during the first 20 ms after the sudden change in sliding velocity, there is practically no change in the shape of the curve of force vs. time.

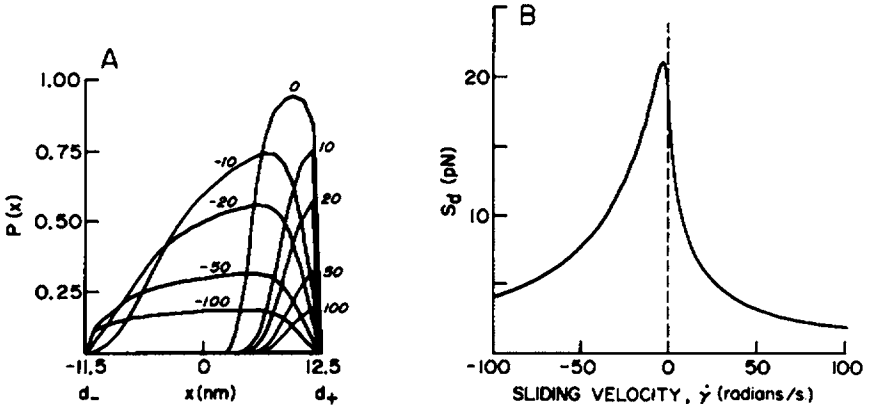

FIGURE 6 Steady-state probabilities and forces as a function of sliding velocity. The positive curvature rate functions given in Fig. 5 were used to compute the probabilities of attachment of one system of dyneins for x values from d_- to d_+ (panel A). The rates of sliding, γ, in radians per second, are as shown. The force-velocity curve in part B was obtained by integrating the probability distribution with $F_a = -k_d(x - x_0)$, with $k_d = 0.4$ pN/nm and $x_0 = -7.64$ nm, according to Eq. 6, and $d_{arm} = d_{att} = 24$ nm.

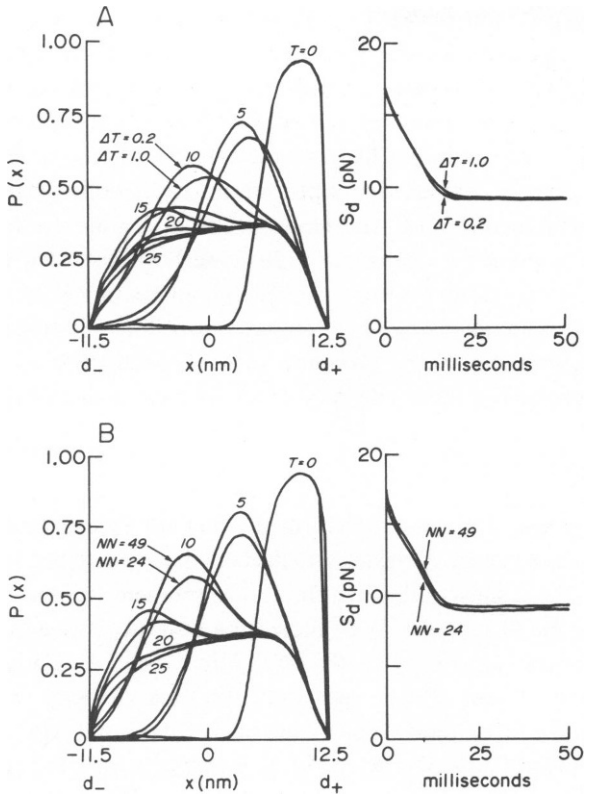

FIGURE 7

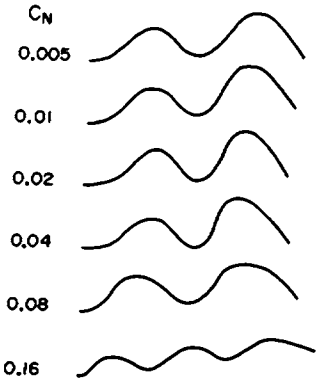

FIGURE 8

FIGURE 7 Transient probabilities and forces for different computational parameters. The steady-state probability distribution for positive curvature at zero sliding velocity, $\dot{\gamma}$, is shown at $t = 0$. At $t = 0$, $\dot{\gamma}$ is suddenly changed to $\dot{\gamma} = -40$ rad/s, and held constant at this value. Probability distributions are shown at 5-ms intervals until a new steady-state distribution is reached. The transient forces are also shown as a function of time. In panel A the probabilities and forces computed using two different Δt steps are overlaid; $NN = 24$ for these computations. In panel B, the probabilities and forces computed using two different values of NN are overlaid; Δt was 0.2 ms. In both panels there was no appreciable further change in probability distribution for times >25 ms. Rate functions are as in Fig. 5.

FIGURE 8 Effect of increasing viscosity on wave shape. Single snapshots taken at roughly comparable stages in the beat cycle (after the transients have subsided) are shown for a 32-fold range of viscosity ($C_N = 0.005$ to 0.16 pN s/μm^2). For these simulations the following parameter values were used: rate functions as in Fig. 5; d, d_{arm}, and $d_{att} = 24$ nm; $L = 30$ μm; $C_T = 0.5\ C_N$; $E_b = 25$ pN μm^2; $A_1 = 15$ pN; $k_d = 0.4$ pN/nm; $N = 40$ ($\Delta s = 0.75$ μm); $NN = 24$ ($\Delta x = 0.96$ nm); $\Delta t = 0.2$ ms; two iterations per time step; $x_0 = -7.64$ nm.

Similarly, if Δt is increased from 0.2 to 1.0 ms, the computed probabilities differ during the transient, but there is no appreciable effect on the curve of force vs. time. Thus $NN = 24$ and $\Delta t = 0.0002$ s are adequate choices to ensure proper computation of the dynein shear force.

Inspection of the way the probabilities change during the transient shows that the primary effect of decreasing Δx and Δt is to increase the accuracy of computation of the terms due to transport in the equation for S_d. Unfortunately, the computational method used here

would require much smaller values of Δt if one wished to compute the probabilities during the transient state with high accuracy. A Crank-Nicolson procedure will compute the probabilities during the transient accurately with reasonable Δt, but for stable computations it is necessary that $\Delta t < \Delta x/v$. This requirement prevents use of the Crank-Nicolson procedure for computation of dynein shear force during flagellar motion, because very large transient velocities occur. We have devised a computational procedure that is both accurate and stable for all velocities for reasonable values of Δt. However, as it is more accurate than the accuracy of computation of $\dot{\gamma}$ [which is correct to $0(\Delta t)$], we have not used this method because we felt it would yield very little improvement in the computation of the dynein force. It should be noted that although changing Δt from 0.2 to 1.0 ms did not significantly change the computed force (see Fig. 7), we compute with the smaller Δt in the flagellar simulations to follow the changes in $\dot{\gamma}$ from one Δt step to the next with sufficient accuracy.

Simulation of Wave Propagation

A series of simulations for a 32-fold range of C_N were performed using the rate functions described in Fig. 5. Each simulation was run until all transient effects had subsided and then continued for several full beat cycles. Fig. 8 shows the wave shape at a moment in time corresponding to similar positions within the beat cycle. With increasing viscosity, wave number is maintained approximately constant until $C_N \sim 0.08$ pN s/μm^2, when a relatively abrupt increase in wave number occurs. It can also be seen that, for each viscosity, wave amplitude appears to increase toward the distal end (right-hand side of each snapshot) of the flagellum. This can be seen more clearly in panels A–C of Fig. 9, where a full beat cycle is presented for three values of C_N. The wave starts off at the proximal end of the flagellum at low amplitude and builds to maximal amplitude in about a half to one wavelength and then propagates at approximately constant amplitude to the distal end. In these simulations waves initiate at the proximal end of the flagellum because we made the control by curvature so that $\kappa > 0$ generates negative shear force. Note that in these simulations sliding is prevented at the proximal end of the flagellum by adding a large value (−2,000 pN) to the elastic shear force, K_{s2}, near the base (see I for details).

Panels D, E, and F of Fig. 9 show the variation in $\dot{\alpha}$ at two successive time steps 0.005 s apart. It can be seen that at low viscosity, $\dot{\alpha}$ contains noticeable error at the flagellum ends. That is, oscillations with a frequency of about $1/\Delta t$ occur. This is because the Crank-Nicolson procedure ensures only that oscillations due to error at a single time step damp out in successive time steps. Because error is always introduced at each time step, oscillations can be eliminated only by use of a fully implicit method. These oscillations do not, however, affect the smoothness of the shape of the flagellum (see panels A, B, and C) because the error in $\dot{\alpha}$ produces only a very small error in α at each time step. Except for the few points at each end, $\dot{\alpha}$ is essentially free of these error oscillations. Notice that for a viscosity about that of water ($C_N = 0.005$ pN s/μm^2) the maximum value of $\dot{\alpha}$ is about 300 rad/s, which corresponds to a shear rate of about $6\Delta x$ per Δt step. This large shear rate justifies the use of the implicit computational procedure for computing the dynein probabilities, because it is unconditionally stable even though of only first-order accuracy.

Panels G, H, and I of Fig. 9 show the influence of viscosity on S_d as a function of arc length for the same times as $\dot{\alpha}$ in panels A, B, and C. As viscosity increases, each dynein

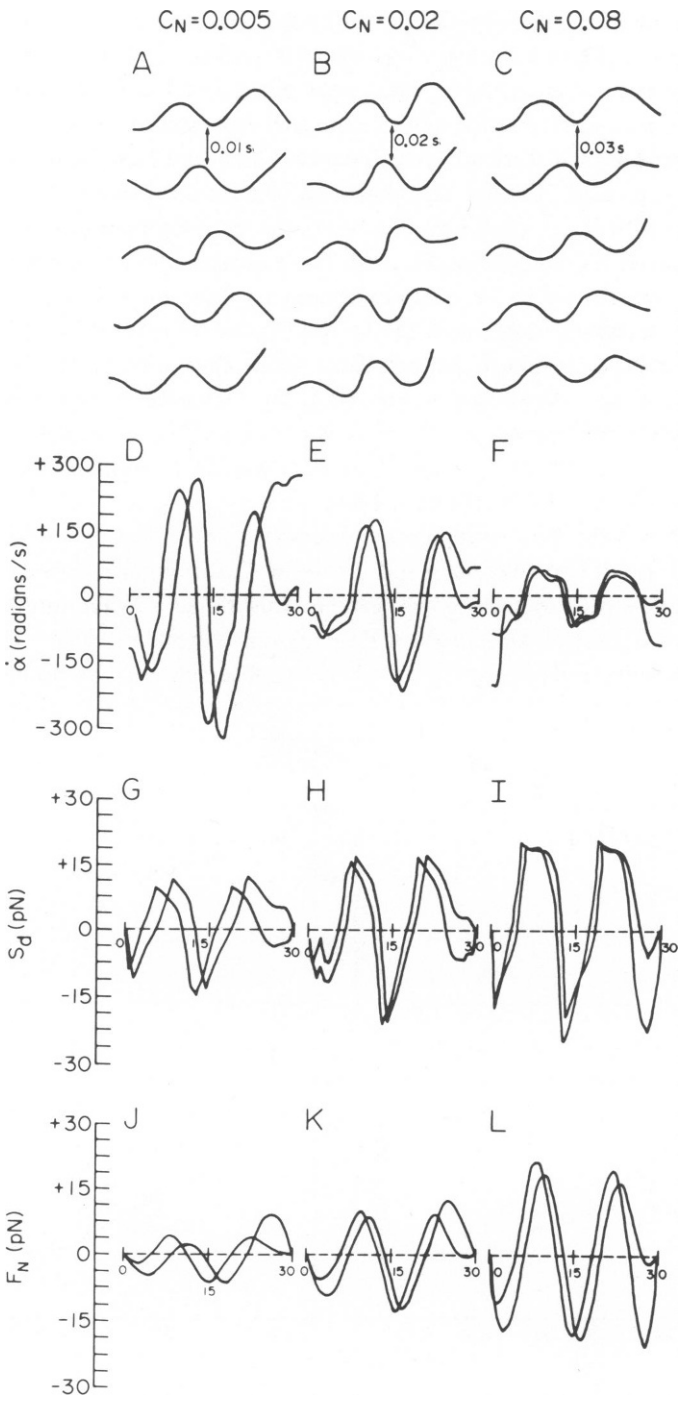

FIGURE 9 Effect of increasing viscosity on wave propagation, $\dot{\alpha}$, S_d, and F_n. In panels A, B, and C enough snapshots of the flagellum are shown to cover one full beat cycle at the indicated values of C_N. Note that the time interval between successive snapshots is indicated in the panels. Successive snapshots are displaced downward for clarity. The abscissa in panels D through L give the arc lengths, s (in μm) and, in each panel, two functions at times 0.005 s apart are presented. Panels D, E, and F present $\dot{\alpha}$; G, H, and I present S_d; and J, K, and L present F_N. Parameter values are as in Fig. 8.

system generates more shear force, thus enabling the flagellum to maintain large amplitude waves with only a moderate decrease in frequency. Clearly, as C_N increases the dynein systems operate more and more closely to the peak of the force-velocity curve in Fig. 6 B, even though a varying $\dot{\gamma}(s, t)$ prevents the dynein systems from ever being in the steady state.

Panels J, K, and L of Fig. 9 are the same as panels G, H, and I except that the viscous normal shear force is plotted. Careful examination of these curves shows that at low viscosity S_d is out of phase with F_N (cf. panels G and J). As the viscosity increases, S_d and F_N become more nearly in phase (cf. panels I and L). At low viscosities, most of the shear force generated by the dyneins is used in overcoming the internal shear and elastic bending resistances; relatively little of the shear force generated by the dynein system is dissipated in the viscous medium. With increasing viscosity enough extra shear force is generated by the dynein system to maintain shape. As shown in Fig. 10 A, F_N increases more rapidly than S_d can mobilize extra shear force until, at $C_N \sim 0.08$ pN s/μm^2, F_N overtakes S_d, after which a change in wave number occurs. Abrupt changes in waveform with viscosity have been observed in flagella of *Ciona* sperm (Brokaw, 1966).

Fig. 10 also shows the effect of increasing viscosity on wavelength, wave amplitude, beat frequency, wave speed, and swimming speed. As in *Ciona* and *Lytechinus* wavelength decreases only slightly with increasing viscosity in this range. Wave amplitude, however, actually increases slightly, as observed for *Chaetopterus* (Brokaw, 1966). Wave speed and frequency decrease in roughly the same ranges as observed for the above three species.

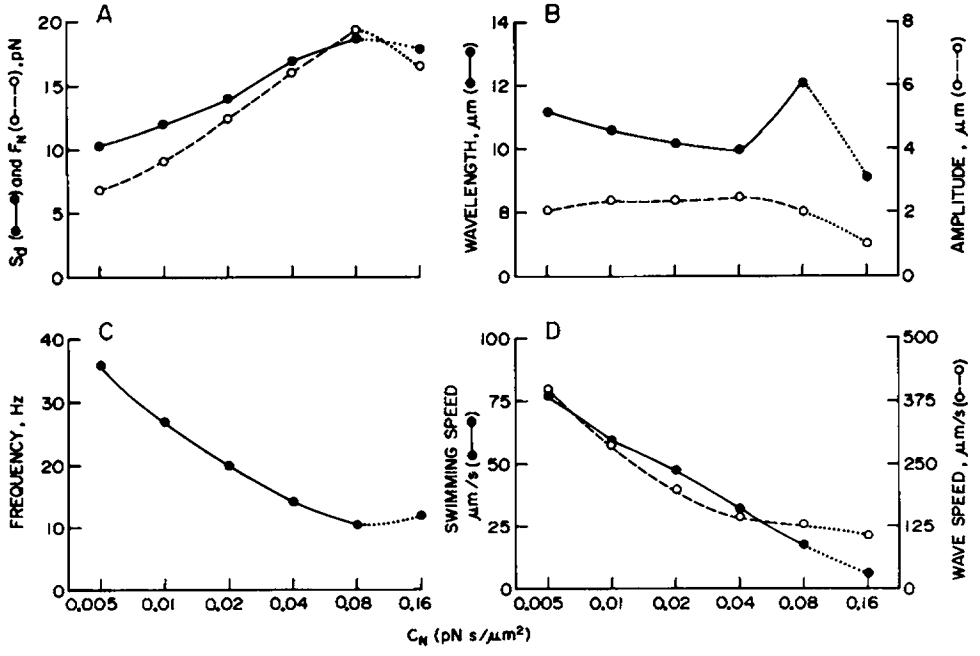

FIGURE 10 Effect of viscosity on wave parameters. C_N, proportional to viscosity ($C_N = 0.005$ pN s/μm^2 corresponds to about 1 cP), is plotted on a logarithmic scale on each abscissa. Because there is a change in mode (see Fig. 8) between $C_N = 0.08$ and $C_N = 0.16$ pN s/μm^2, the curves are drawn with a dotted line in this interval. Panel A shows the maximum values of $S_d(s, t)$ and $F_N(s, t)$, respectively. Parameter values are as in Fig. 8.

Swimming speed decreases from ~80 to ~17 μm/s as the viscosity increases 32-fold above that of water. A similar decrease in swimming speed has been observed for *Polytoma uvella* (Brokaw, 1962).

DISCUSSION

In the present paper a model has been developed for dynein arm attachment and detachment during flagellar motion. Although the model developed is in principle easily extended to more realistic dynein cross-bridge diagrams, we have in this paper confined ourselves to a two-state diagram and have assumed that the dynein arms do not compete for attachment sites and have only one attachment site available at any instant of time. Current electron microscope evidence indicates that dynein arms attach at an angle of about 30° and detach when approximately perpendicular (Sale and Satir, 1977; Warner and Mitchell, 1978), consistent with the view that dynein arms do not compete for the same sites. It is not yet clear, however, whether multiple attachment sites are available to a single dynein arm, as the fundamental repeat distance of tubulin dimers in microtubules is 8 nm (Gibbons, 1977), and it is not known how many repeat distances separate attachment sites. It would be unwarranted to investigate a multiple site system at this stage.

Incorporation of a dynein cross-bridge formalism into the equations of motion of a flagellum required solution of two problems that had not arisen in our earlier effort. The first was, given $\dot{\alpha}$, how to compute the dynein shear force, S_d. Computation of S_d requires computation of the probabilities of attachment. Stability requires that one integrate in the proper direction and that the probabilities be kept in the range 0–1 for any value of the sliding velocity, $\dot{\gamma}$. The Crank-Nicolson method, although formally stable, allows the occurrence of negative probabilities for large $\dot{\gamma}$. This, when coupled into the equations of motion, leads to instability. This difficulty may be circumvented by using a fully implicit method for solution of the probability equations. This leads to some inaccuracy in the computation of $P(x)$ but, as discussed above, very little error in the computation of S_d. A consequence of this approach is that some error may arise during calculation of the transient motion from the initial condition to the steady state. It will be recalled that in the previous paper, where it was easy to compute S_d to second order, good accuracy was attainable even during the transient state, and we were able to compare solutions at identical times with different values for the numerical parameters; thus we were able to claim quantitative validity for the computations. With the probabilistic dynein system, however, only semiquantitative accuracy is obtained; one cannot compare shapes at identical times after a long time has elapsed, but instead must compare beat cycles. It must be emphasized, however, that, as can be seen from Fig. 4, the computations here presented are entirely adequate.

In the previous paper (I) we suggested that dynein bridges could be added to the dynamic equations in a straightforward manner because S_d would be a time-delayed function of the shape and there would be no problems of computational stability of the difference equations. In fact, however, the transport of dynein arms due to sliding is the dominant term in the computation of S_d. Because S_d to a large extent determines the amount of sliding in a time step, one must compute both $\dot{\gamma}$ and S_d simultaneously. They are coupled so strongly, however, that a simple iterative procedure which computes one and then the other will not converge for reasonable values of Δt. Fortunately, the method devised in the previous paper

for computation of S_r, the contribution of the radial link system to the shear force, could be generalized to the dynein cross-bridge system. Specifically, S_d could be resolved by a variational procedure into terms linearly proportional to γ and other terms, thereby allowing a convergent iterative procedure for simultaneous evaluation (via a matrix inversion) of both S_d and $\dot{\gamma}$.

In the previous paper, τ, the time delay of the formal analogue of the dynein system, was about 0.01 s, i.e. an order of magnitude larger than the computational Δt (0.001 s) and thus the dynein force could be tracked accurately. The introduction of a dynein cross-bridge system automatically means that the basic unit of time is the time required for the dynein arm to move from a position with one probability of attachment to a position with a noticeably different probability of attachment and of force production. Call the distance involved Δx. Because we assume that an effective attachment-detachment cycle occurs within a region 24 nm long, and we felt that significant changes in attachment probabilities and forces would occur in nanometer intervals, we chose $NN = 24$, so that $\Delta x \sim 1$ nm. For a flagellum beating at 30 Hz, a half cycle requires about $1.67 \cdot 10^{-2}$ s. Thus $\dot{\gamma}$ is about 2 rad/$1.67 \cdot 10^{-2}$ s, or ~ 120 rad/s. Sliding velocity, $\dot{x}$ ($= \pm 0.75 h \dot{\gamma}$), is then about 3,600 nm/s. To follow a change 1 nm therefore requires a Δt of about $2.8 \cdot 10^{-4}$ s, consistent with the value $\Delta t = 2 \cdot 10^{-4}$ s used in the present simulations. Use of this small value of Δt, required for accuracy of computation, in conjunction with the necessity of solving the partial differential Eq. 9 at NN values of x for N segments of arc length Δs, is computationally costly. For example about 4.5 s of IBM 370 CPU time is required to compute 0.01 s of flagellar motion.

As mentioned earlier we have considered only a two-state dynein diagram. Even within these confines, however, we have not made a systematic search of the various parameters that entered into the rate equations, nor have we considered other possible rate functions. In part this was dictated by the large cost of such an investigation, but the more fundamental reason is that it is highly unlikely that a two-state diagram is an adequate representation of the mechanochemical behavior of dynein arms. It seems certain that at least a three-state diagram will be necessary if the ATP dependence of flagellar motility is to be adequately modeled (Brokaw and Rintala, 1977); recent studies indicate that a four-state diagram is the minimum for satisfactory description of the transient as well as the isotonic properties of muscle (Eisenberg and Hill, 1978). It seems more economical, therefore, to proceed to analysis of a realistic dynein diagram rather than attempting to refine the two-state system.

Some general comments on the effects of varying the parameters in the two-state model are, however, worth mentioning. Raising k_d from 0.4 to 0.8 pN markedly reduces wave amplitude, wave speed, and frequency. This is a consequence of the very large decrease in probability of attachment because of the shift of $f'(x)$ toward x_0 (see Eq. 21a). If k_d is kept at 0.4 pN, increasing f_0 and g_0 in Eq. 20 will increase frequency with relatively little change in wave shape. Increasing E_b decreases wave number (discontinuously, i.e., via changes in mode). Increasing A_1 decreases the amount of sliding that occurs and hence decreases wave amplitude.

Despite the lack of any serious attempt to obtain the "best" parameters for the rate functions of the two-state diagram, the results obtained with the present rate functions reproduce the basic features of flagellar motility as a function of viscosity. In sperm of *Ciona*,

Chaetopterus, and *Lytechinus*, frequency decreases <4-fold with a 32-fold rise in viscosity. Such a small decrease in frequency with increasing load requires a dynein system with a large reserve capacity. It is gratifying that even a two-state dynein cross-bridge model has this reserve capacity. Experimentally, there is a considerable range of variation in the effect of viscosity on curvature. In sperm of *Chaetopterus*, for example, wavelength decreases four-fold, whereas curvature actually increases as viscosity increases. Because intuitively one expects a decrease in wave amplitude and curvature with increasing viscosity, as observed in sperm of *Ciona* and *Lytechinus* (Brokaw, 1966), we anticipated that the behavior of *Chaetopterus* might require a more realistic dynein diagram or a complex control system stabilizing wavelength and curvature. As it turns out, however, even a two-state diagram and an exceedingly simple curvature-control system simulates this behavior. We thus conjecture that enough latitude is available within the confines of a two-state curvature-dependent diagram to model the effect of viscosity in sperm which generate planar bending waves.

In this and all previous studies, control of bend propagation by curvature has been introduced in an entirely arbitrary fashion. According to the data of Warner and Satir (1964), the radial link system may play a key role in the control of bend propagation. It would be desirable, however, to have further experimental information before attempting to construct a cross-bridge formalism for the radial links. It is an open question whether bend propagation can be attained without some type of control by curvature.

APPENDIX A

The error accompanying the evaluation of the probabilities in Eqs. 9 can be assessed as follows. Consider the Taylor series expansion, correct to order Δt and to order $v\Delta x$.

$$\frac{\partial P}{\partial t} + v\frac{\partial P}{\partial x} = \frac{P(x, t + \Delta t) - P(x, t)}{\Delta t} + 0(\Delta t) + v\frac{P(x, t + \Delta t) - P(x - \Delta x, t + \Delta t)}{\Delta x} + 0(v\Delta x) = F(x) - G(x)P(x, t + \Delta t). \tag{A1}$$

Solving for $P(x, t + \Delta t)$, one obtains

$$P(x, t + \Delta t) = \frac{P(x, t)/\Delta t + (v/\Delta x)\, P(x - \Delta x, t + \Delta t) + F(x) + 0(v\Delta x) + 0(\Delta t)}{1/\Delta t + v/\Delta x + G(x)}. \tag{A2}$$

Suppose $P(x - \Delta x, t + \Delta t)$ equals the true value of P plus an error term, $E(x - \Delta x, t + \Delta t)$. Then the error in $P(x, t + \Delta t)$ caused by advancing from t to $t + \Delta t$ is

$$E(x, t + \Delta t) = \frac{v\Delta t E(x - \Delta x, t + \Delta t)/\Delta x + 0(v\Delta x\Delta t) + O(\Delta t^2)}{1 + v\Delta t/\Delta x + G(x)\Delta t}. \tag{A3}$$

For small v, the error is of order $\Delta t^2 + v\Delta x\Delta t$ and therefore the total accumulated error over a finite interval of time is order $\Delta t + v\Delta x$. For large v,

$$E(x, t + \Delta t) \sim E(x - \Delta x, t + \Delta t) + 0(\Delta x^2) + \Delta x/v0(\Delta t). \quad \text{(A4)}$$

Because the range of x values is finite, the maximum error, $E(x, t)$, is of order $\Delta x + 1/v\Delta t$, and the accumulated error over a finite time interval is then of order $(\Delta x/\Delta t + 1/v)$ which, for extremely large v, is $0(\Delta x/\Delta t)$.

To assess the error accompanying numerical evaluation of the total derivative form of Eq. 9, one can write a second-order correct difference equation for Eq. 9, assuming v to be known during a time step, as

$$\frac{P(x + 0.5v\Delta t, t + 0.5\Delta t) - P(x, t)}{0.5\Delta t} = F(x + 0.5v\Delta t) - G(x + 0.5v\Delta t)P(x + 0.5v\Delta t, t + 0.5\Delta t), \quad \text{(A5)}$$

for the first half-time step. The second half-time step may then be performed explicitly via $P(x + v\Delta t, t + \Delta t) = 2P(x + 0.5v\Delta t, t + 0.5\Delta t) - P(x, t)$. We desire to know how accurately the left-hand side of A5 represents dP/dt. As the Taylor series expansion of $P(x + v\Delta t, t + \Delta t)$ about $x + 0.5v\Delta t$ and $t + 0.5\Delta t$ is

$$P(x + v\Delta t, t + \Delta t) = P(x + 0.5v\Delta t, t + 0.5\Delta t) + 0.5\Delta t \frac{\partial P}{\partial t} + 0.5v\Delta t \frac{\partial P}{\partial x} + \frac{(0.5\Delta t)^2}{2} \frac{\partial^2 P}{\partial t^2} + \frac{(0.5v\Delta t)^2}{2} \frac{\partial^2 P}{\partial x^2} + v(0.5\Delta t)^2 \frac{\partial^2 P}{\partial x \partial t} + \left(0.5\Delta t \frac{\partial}{\partial t} + 0.5v\Delta t \frac{\partial}{\partial x}\right)^3 P + \cdots, \quad \text{(A6)}$$

it can easily be shown that

$$\frac{dP}{dt}_{x+0.5v\Delta t, t+0.5\Delta t} = \frac{P(x + v\Delta t, t + \Delta t) - P(x, t)}{\Delta t} + (\Delta t^2 + v^3\Delta t^2). \quad \text{(A7)}$$

Although the transport of the dynein arms from their original positions to their final positions is performed exactly if v is exactly known, the attachments and detachments possible along the way are not accurately accounted for if $v \gg \Delta x/\Delta t$. The error arising from this uncertainty can be considerably larger than the error arising during numerical evaluation of the partial differential equation.

This work was supported by National Institutes of Health grant 1 R01 NS11613, as was the preceding paper of this series.

Received for publication 29 June 1978 and in revised form 31 October 1978.

REFERENCES

1. Brokaw, C. J. 1962. Studies on isolated flagella. *In* Spermatozoan Motility. D. W. Bishop, editor. American Association for the Advancement of Science, Washington, D.C. 269.
2. Brokaw, C. J. 1966. Effects of increased viscosity on the movements of some invertebrate spermatozoa. *J. Exp. Biol.* **45**:113.
3. Brokaw, C. J. 1975*a*. Computer simulation of flagellar movement. III. Models incorporating cross bridge kinetics. *J. Mechanochem. Cell Motility.* **3**:77.

4. BROKAW, C. J. 1975*b*. Molecular mechanism for oscillation in flagella and muscle. *Proc. Natl. Acad. Sci. U. S. A.* **72**:3102.
5. BROKAW, C. J. 1976*a*. Computer simulation of movement generating cross-bridges. *Biophys. J.* **16**:1013.
6. BROKAW, C. J. 1976*b*. Computer simulation of flagellar movement. IV. Properties of an oscillatory two-state cross-bridge model. *Biophys. J.* **16**:1029.
7. BROKAW, C. J. 1977. Is the 9 + 2 pattern of flagellar and ciliary axonemes an efficient arrangement for generating planar bending? *J. Mechanochem. Cell. Motility.* **4**:101.
8. BROKAW, C. J., and D. RINTALA. 1977. Computer simulation of flagellar movement. V. Oscillation of cross-bridge models with an ATP-concentration-dependent rate function. *J. Mechanochem. Cell Mobility.* **4**:205.
9. BLUM, J. J., and A. HAYES. 1977. A comparison of the effects of gentle heating, acetone, and the sulfhydryl reagent bis(4-fluoro-3-nitrophenyl) sulfone on the ATPase activity and pellet height response of *Tetrahymena* cilia. *J. Supramol. Struct.* **6**:155.
10. EISENBERG, E., and T. L. HILL. 1978. A cross-bridge model of muscle contraction. *Prog. Biophys. Mol. Biol.* **33**:55.
11. GIBBONS, I. R. 1977. Structure and function of flagellar microtubules. *In* International Cell Biology, 1976–1977. B. R. Brinkley and K. R. Porter, editors. Rockefeller University Press, New York. 348.
12. HILL, T. L. 1974. Theoretical formalism for the sliding filament model of contraction of striated muscle. Part I. *Prog. Biophys. Molec. Biol.* **28**:267.
13. HILL, T. L. 1975. Theoretical formalism for the sliding filament model of contraction of striated muscle. Part II. *Prog. Biophys. Molec. Biol.* **29**:105.
14. HILL, T. L., E. EISENBERG, Y. CHEN, and R. J. PODOLSKY. 1975. Some self consistent two-state sliding filament models of muscle contraction. *Biophys. J.* **15**:335.
15. HINES, M., and J. J. BLUM. 1978. Bend propagation in flagella. I. Derivation of equations of motion and their simulation. *Biophys. J.* **23**:41.
16. LUBLINER, J., and J. J. BLUM. 1971. Model for bend propagation in flagella. *J. Theor. Biol.* **31**:1.
17. SALE, W. S., and P. SATIR. 1977. Direction of active sliding in *Tetrahymena* cilia. *Proc. Natl. Acad. Sci. U. S. A.* **74**:2045.
18. WARNER, F. D., and P. SATIR. 1974. The structural basis of ciliary bend formation: radial spoke positional changes accompanying microtubule sliding. *J. Cell Biol.* **63**:35.
19. WARNER, F. D., and D. R. MITCHELL. 1978. Structural conformation of ciliary dynein arms and the generation of sliding forces in *Tetrahymena* cilia. *J. Cell Biol.* **76**:261.